High-Resolution ^{13}C NMR Configurational Analysis of Polypropylene Made with $MgCl_2$-Supported Ziegler−Natta Catalysts. 1. The "Model" System $MgCl_2/TiCl_4$−2,6-Dimethylpyridine/$Al(C_2H_5)_3$

Vincenzo Busico,* Roberta Cipullo, Guglielmo Monaco, Giovanni Talarico, and Michele Vacatello

Dipartimento di Chimica, Università di Napoli "Federico II", Via Mezzocannone, 4, 80134 Napoli, Italy

John C. Chadwick

Montell Polyolefins, Centro Ricerche "Giulio Natta", Piazzale Donegani, 12, 44100 Ferrara, Italy

Anna Laura Segre

Istituto di Strutturistica Chimica e Servizio NMR del CNR, Area della Ricerca di Roma, C.P. 10, 00165 Monterotondo Stazione, Italy

Olof Sudmeijer

Shell Research and Technology Centre, Amsterdam (Shell International Chemicals, B.V.), P.O. Box 38000, 1030 BN Amsterdam, The Netherlands

Received December 17, 1998; Revised Manuscript Received March 26, 1999

ABSTRACT: The stereosequence distribution of the "atactic" and "isotactic" fractions of a polypropylene sample made with a $MgCl_2$-supported catalyst was determined by means of high-resolution ^{13}C NMR and analyzed in terms of statistical models of increasing sophistication. Two-site models, including the one normally used for the interpretation of "routine" ^{13}C NMR data at pentad level, were shown to be inconsistent with the much finer high-resolution data. A good agreement between experimental and calculated distributions could be obtained only in terms of a three-site model, describing each fraction as a mixture of highly isotactic, weakly isotactic ("isotactoid") and syndiotactic sequences. According to such model, the two fractions comprise the same three building blocks (the configuration of the three different types of stereosequences being almost invariant) and differ merely in their relative amounts (which indicates a stereoblock nature). The correlations with the physical properties of the materials and the implications on the nature of the catalytic species are also briefly discussed.

Introduction

In recent papers,[1,2] some of us have reported the complete assignment of the 150 MHz ^{13}C NMR spectra of regioregular polypropylenes of different tacticities and shown that the configuration of such polymers can now be elucidated at the heptad/nonad level in a relatively straightforward manner even for samples of poor stereoregularity. This resulted, inter alia, in a major improvement of the methods for the stereochemical investigation of the polymerization reactions based on the statistical analysis of polymer microstructure.[1,3−8]

In such a context, the "classical" heterogeneous Ziegler−Natta systems (either $TiCl_3$-based[9−11] or $MgCl_2$-supported[10−12]) still represent the most challenging application. These catalysts are known to contain different classes of active species, some of which undergo reversible interconversions; as a result, they afford polypropylenes which are complicated mixtures of highly isotactic, poorly isotactic ("isotactoid"), and syndiotactic sequences, at least in part chemically linked to form stereoblock chains.[1,5−14]

A rough but practical method for evaluating the stereoregularity of a given polymer sample is to measure the weight fraction that is insoluble in a certain solvent under certain conditions and as such is conventionally referred to as "isotactic".[9−11] Two popular (and substantially equivalent) procedures are extraction with boiling heptane and crystallization from xylene solution. Although it is well-known that polymer solubility depends on the molecular mass as well, it is commonly assumed that in the range of average molecular masses of commercial grade polypropylenes this dependence is only marginal and that the fractionation is mainly governed by tacticity;[9−14] as a matter of fact, typical "isotactic" fractions (i.e., heptane- or xylene-insoluble) have a content of *mmmm* pentads (measured by ^{13}C NMR) in excess of 90%.[8,13g,h]

The polymer fraction soluble in boiling heptane or in xylene at room temperature, in turn, is often referred to as "atactic", although it has long been recognized that this notation is not appropriate. Indeed, no truly atactic chains are found in such fraction, which contains instead isotactoid and syndiotactic sequences.[1,5−8,13,14]

It is also well-known that, by extracting heptane-soluble fractions with lower boiling solvents (such as diethyl ether, pentane, or hexane)[1,5,13f] or by means of temperature rising elution fractionation,[14] minor amounts of weakly crystalline subfractions can be separated from an amorphous part. ^{13}C NMR indicates that the latter is unable to crystallize due to the combined effects of a poor stereoregularity and of a low average length of the (predominantly) isotactic and syndiotactic blocks.

Quite surprisingly, however, recent ^{13}C NMR investigations proved that most "isotactic" fractions are also

10.1021/ma981941n CCC: $18.00
Published on Web 06/11/1999

stereoblock materials, in which very long blocks of almost ideal isotacticity are spanned by short syndiotactic blocks.[1b,8,13h,14c−e]

Thus, it is now being realized that the difference between "isotactic" and "atactic" polypropylene is less clear-cut than has been assumed and that the mechanisms of stereocontrol leading to their formation are intimately related.

In this paper, we present the results of a *comparative* high-resolution ^{13}C NMR microstructural analysis of an "atactic" and an "isotactic" polypropylene fraction prepared with a suitable $MgCl_2$-supported catalyst, from which we derive new insight into the structure of the polymer and, correspondingly, into the behavior of the catalytic species. A preliminary, partial account of this study was presented in refs 1d,e.

Results and Discussion

Choice of the Polypropylene Fractions. The stereoselectivity of $MgCl_2$-supported systems is a function of the specific Lewis bases used as components of the solid catalyst ("internal donors") or added in combination with the Al−alkyl cocatalyst ("external donors").[11,12]

It is common practice to evaluate the effectiveness of catalyst modification by a certain combination of internal and external donors in terms of the resulting value of the "isotacticity index" (I.I.; weight fraction of polymer insoluble in boiling heptane) or of the "xylene index" (X.I.; weight fraction of polymer insoluble in xylene at room temperature).[11,12] Industrial catalysts are characterized by I.I. and/or X.I. values higher than 95%.[12]

However, Lewis bases affect not only the balance between "isotactic" and "atactic" fraction but also, to some extent, their microstructure.

A distinctive feature of "isotactic" fractions made with latest-generation industrial catalysts, such as those modified with dialkyl phthalates and alkoxysilanes[12d−i] or with 1,3-diethers,[12j] is a low content (<1−2 wt %) of syndiotactic blocks.[1b,8,13g,h,14c−e] This feature, coupled with a very high stereoregularity of the isotactic blocks, results in a DSC melting temperature T_m > 165 °C and in the fact that a substantial part of the material is insoluble even in boiling octane.[12e,13g,h]

"Atactic" fractions also show a certain stereochemical variability. In particular, the addition of an external donor tends to increase the relative amount of syndiotactic sequences,[13f] which in a few special cases can even become predominant.[1d]

For our investigation, we selected a diethyl ether-insoluble/pentane-soluble fraction (A) and a xylene-insoluble fraction (B) of a polypropylene sample prepared in the presence of the catalyst system $MgCl_2$/$TiCl_4$−2,6-dimethylpyridine/Al(C_2H_5)$_3$. This system is peculiar in that it affords polypropylenes with relatively high contents of crystallizable syndiotactic sequences both in the "atactic" and in the "isotactic" fraction; therefore, in the statistical analysis of polymer configuration, it can be assumed that the average length of such sequences is high enough to neglect the possible presence of block junctions, which would represent a major source of complication.

We also checked that in both fractions the concentration of chain end groups is below the limit for ^{13}C NMR detectability (M_v = 1.5 × 10^5 Da for fraction A, 5.7 × 10^5 Da for fraction B).

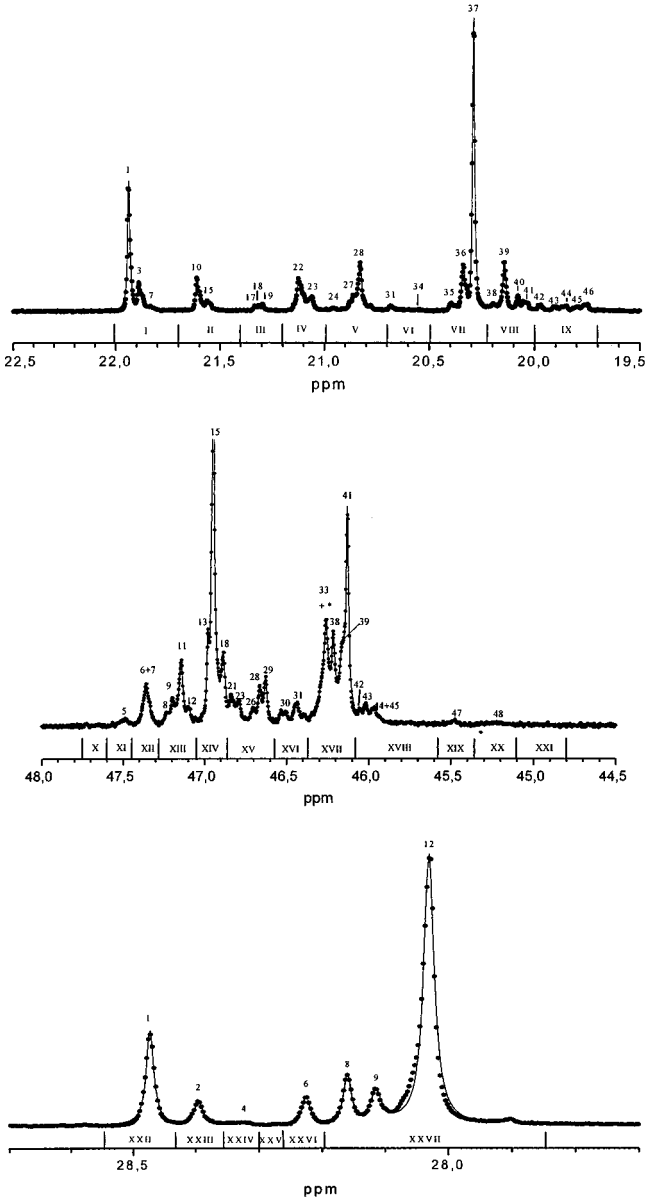

Figure 1. Experimental (dotted) and simulated (solid) 150 MHz ^{13}C NMR spectrum of fraction A (in tetrachloroethane-*1,2-d*$_2$ solution at 70 °C). The δ scale is in ppm downfield of TMS; peak and range numbering refers to the full assignment reported in ref 2. (a, top) Methyl region; (b, middle) methylene region; (c, bottom) methine region.

In a forthcoming paper, we will show that the conclusions reached on these "model" polypropylenes can be extended to polymers made with typical industrial catalysts.

Configurational Analysis of the "Atactic" Fraction A. The 150 MHz ^{13}C NMR spectrum of fraction A at 70 °C is shown in Figure 1. Peak numbering refers to the full assignment given in ref 2.

The spectrum was simulated by means of a convenient set of Lorentzian functions:[15] the resulting complex least-squares fit[15a] is also shown in the figure. Such a fit is obviously an approximation, mainly because the complete fine structure at nonad/undecad level is not accessible even at 150 MHz; this means that not all individual Lorentzians can be associated with a specific steric *n*ad or even to a collection of *n*ads.

As an example, the main contributions to methyl peaks 1, 3, and 7 (Figure 1a) derive unquestionably from

Table 1. Stereosequence Distribution of Fraction A (for the Definition of the Adjustable Parameters, See Text)

		normalized fraction								
range/peak no.	assignment	expl	calcd, ES/CE		calcd, C_1/CE		calcd, ES/C_1/CE (general)		calcd, ES/C_1/CE (constrained)	
I	*mmmm*	0.1937(50)	0.2110		0.2015		0.1971		0.1971	
XXII	*mmmmmm*	0.1514(38)	0.1532		0.1424		0.1514		0.1514	
XXIII	*mmmmmr*	0.0389(35)	0.0531		0.0538		0.0390		0.0389	
II	*mmmr*	0.0708(29)	0.0746		0.0770		0.0711		0.0712	
XXVI/6	*mmmmrr*	0.0426(33)	0.0532		0.0627		0.0508		0.0508	
III	*rmmr*	0.0141(31)	0.0121		0.0131		0.0161		0.0161	
III/17	*mrrmmrrm*	0.0042(15)	0.0034		0.0047		0.0056		0.0056	
III/18	*mrrmmrrr*	0.0044(22)	0.0019		0.0034		0.0055		0.0055	
IV	*mmrr*	0.0999(32)	0.0828		0.0993		0.0995		0.0995	
IV/22	*mmmrrm* + *mmmrrr*	0.0709(22)	0.0633	0.0532 0.0101	0.0748	0.0578 0.0170	0.0688	0.0474 0.0214	0.0688	0.0473 0.0215
V	*mmrm* + *rmrr*	0.1048(79)	0.1104	0.0159 0.0945	0.0983	0.0039 0.0944	0.1026	0.0040 0.0986	0.1025	0.0039 0.0986
V/24	*mmmrmr*	0.0030(15)	0.0094		0.0019		0.0022		0.0023	
VI	*rmrm*	0.0110(16)	0.0241		0.0128		0.0121		0.0121	
VI/31	*rrmrmr*	0.0090(10)	0.0093		0.0082		0.0071		0.0071	
VI/34	*mrmrmm*	0.0010(10)	0.0094		0.0019		0.0021		0.0021	
VII	*rrrr*	0.3423(47)	0.3492		0.3493		0.3494		0.3493	
VII/37	*rrrrrr*	0.2736(36)	0.2752		0.2677		0.2674		0.2674	
VIII/38	*mrrrmr*	0.0086(13)	0.0093		0.0083		0.0073		0.0073	
VIII/39	*rrrrmr*	0.0665(15)	0.0657		0.0671		0.0642		0.0642	
VIII/40+41	*rrrrmm* + *mrrrmm*	0.0364(30)	0.0194	0.0167 0.0027	0.0283	0.0269 0.0014	0.0348	0.0332 0.0016	0.0347	0.0331 0.0016
IX/42	*rmrrmr*	0.0090(15)	0.0047		0.0046		0.0055		0.0054	
IX/43+44	*mmrrmr*	0.0189(36)	0.0101		0.0099		0.0161		0.0162	
IX/45+46	*mmrrmm*	0.0248(36)	0.0266		0.0306		0.0243		0.0243	
X	*mrmrm*	0.0006(15)	0.0060		0.0016		0.0017		0.0017	
XI	*mrmrr*	0.0077(15)	0.0120		0.0096		0.0086		0.0086	
XII	*rrmrr* + *mrrrm*	0.0486(7)	0.0472	0.0412 0.0060	0.0473	0.0424 0.0049	0.0494	0.0450 0.0044	0.0494	0.0450 0.0044
XIII+ XIV+ XV	*mrrrr* + *rmmrm* + *rrrrr* + *rmmrr* + *mmmrm* + *mmmrr*	0.4946(52)	0.4892	0.0826 0.0047 0.3080 0.0194 0.0112 0.0633	0.4995	0.0940 0.0018 0.3023 0.0245 0.0021 0.0748	0.5015	0.0975 0.0016 0.3006 0.0307 0.0023 0.0688	0.5015	0.0976 0.0016 0.3006 0.0306 0.0023 0.0688
XIII/9	*mmrrrrm*	0.0200(12)	0.0086		0.0157		0.0194		0.0195	
XIII/11	*rmrrrrr*	0.0525(11)	0.0577		0.0580		0.0528		0.0528	
XIX	*rmrmr*	0.0046(15)	0.0060		0.0048		0.0042		0.0042	
XX	*mmrmr*	0.0052(15)	0.0121		0.0033		0.0037		0.0037	
			$\Sigma(y_{i,c} - y_{i,o})^2 \times 10^3 = 2.04$, $\chi_r^2 = 15.9$		$\Sigma(y_{i,c} - y_{i,o})^2 \times 10^3 = 1.25$, $\chi_r^2 = 5.6$		$\Sigma(y_{i,c} - y_{i,o})^2 \times 10^3 = 0.28$, $\chi_r^2 = 1.46$		$\Sigma(y_{i,c} - y_{i,o})^2 \times 10^3 = 0.28$, $\chi_r^2 = 1.40$	
			$\sigma = 0.85$				$\sigma = 0.99_5$			
					$\sigma_1 = 0.98_8$		$\sigma_1 = 1.00$		$\sigma_1 = 1.00$	
					$\sigma_2 = 0.63$		$\sigma_2 = 0.35$		$\sigma_2 = 0.36$	
					$P_{12} = 0.59$		$P_{12} = 0.49$		$P_{12} = 0.48$	
					$P_{21} = 0.99$		$P_{21} = 0.95$		$P_{21} = 0.95$	
			$P_r = 0.90$		$P_r = 0.89$		$P_r = 0.90$		$P_r = 0.90$	
			$w_{ES} = 0.47$				$w_{ES} = 0.10$		$w_{ES} = 0.095$	
					$w_{C_1} = 0.47$		$w_{C_1} = 0.43$		$w_{C_1} = 0.43$	

the *mmmmmm*, *mmmmmr*, and *rmmmmr* heptads, respectively.[2a] However, the peaks are partly overlapped, and any attempt of separate evaluation would be somewhat arbitrary because this would require to locate all constituting longer *n*ads with appreciably different chemical shifts. In this case, we could take advantage of the lucky circumstance that the same three heptads give rise to well-separated peaks in the methine region[2b] (Figure 1c, peaks 1, 2, and 4); in less fortunate cases, however, we decided to use only summed areas and not the strongly correlated individual areas obtained by the complex least-squares fit.

Despite this limitation, which precluded the detailed analysis of large parts of the crowded methylene and methine regions, we were able to extract 31 independent normalized integrals corresponding to a collection of steric *n*ads from pentads to nonads (Table 1, columns 1−3).

The results were then subjected to best-fit calculations[16] in terms of multisite statistical models built as linear combinations of suitable single-site models, starting of course from two-site ones.

The ES/CE Two-Site Model. This now classical model, introduced in the early 1980s,[5] is still widely used for the best fit of the stereosequence distribution of "atactic" polypropylene fractions at the pentad level determined by "routine" ^{13}C NMR.[13,14]

It assumes that such fractions are mixtures of two basic types of stereosequences: predominantly isotactic (or "*m*-rich" or isotactoid) and predominantly syndiotactic (or "*r*-rich" or syndiotactoid). The configuration of the former is described in terms of the "enantiomorphic sites" (ES) statistics[4] and that of the latter in terms of the "chain end" (CE) statistics.[3] The underlying mechanistic implication is that the stereocontrol of isotactic propagation is exerted by intrinsically chiral

transition metal active species, whereas syndiotactic propagation would be due to a 1,3-*unlike* (*ul*) asymmetric induction involving the last-inserted monomeric unit of the growing chain.[11]

When the analysis is limited to the steric pentads, it is possible to apply this model by solving in the least-squares sense the overdetermined set of equations that give the probability of occurrence for each single pentad.[5]

On the other hand, when high-resolution ^{13}C NMR data at the hexad/nonad level are available, this approach becomes highly impractical, and the use of matrix multiplication techniques is advisable. The interested reader is referred to the Appendix of ref 1c, in which we introduced a general formalism for calculating the probability of occurrence of steric *n*ads of any length in the framework of any desired statistical model.

In its original formulation,[4] the enantiomorphic sites model assumes that (i) the catalyst can be described as a racemic mixture of enantiomorphous active sites, (ii) opposite enantiofaces of the prochiral monomer are preferred at sites of opposite chirality, (iii) the configuration of the last-inserted unit has no effect on the enantioselection, and (iv) the chirality of each individual active site is invariant. Under such hypotheses, chain propagation can be described in terms of the following stochastic matrix:

$$\mathbf{E} = \begin{array}{c|cc} & \text{R or S} & \text{S or R} \\ \hline \text{R or S} & \sigma & 1-\sigma \\ \text{S or R} & \sigma & 1-\sigma \end{array}$$

σ and $(1 - \sigma)$ are the conditional probabilities that the two opposite monomer enantiofaces are selected at an active site of given chirality, thus generating monomeric units with opposite configurations. The propagation tends to ideal isotacticity for $\sigma \rightarrow 1$ or $\sigma \rightarrow 0$ and to ideal atacticity for $\sigma \rightarrow 0.5$. In all cases, the resulting distribution of *configurations* is Bernoullian (zero-order Markovian).

The chain-end model,[3] instead, assumes a first-order Markovian distribution of *configurations* with $P_{XY} = P_{YX}$ (X = R or S, Y = S or R), which results in a Bernoullian (zero-order Markovian) distribution of *steric diads*. The corresponding stochastic matrix is

$$\mathbf{C} = \begin{array}{c|cc} & \text{R} & \text{S} \\ \hline \text{R} & 1-P_r & P_r \\ \text{S} & P_r & 1-P_r \end{array}$$

P_r is the conditional probability that monomer insertion gives rise to the formation of a racemic (*r*) diad; of course, $P_r > 0.5$ corresponds to predominantly syndiotactic propagation.

The ES/CE model is a linear combination of the above two single-site models, with mixing coefficients w_{ES} and $(1 - w_{ES})$, respectively.[5]

In the fourth column of Table 1, we report the best-fit stereosequence distribution for fraction A according to this very simple two-site model, along with the corresponding values of the three adjustable parameters σ, P_r, and w_{ES}. If, on one hand, the main features of the experimental distribution (i.e., the occurrence of predominantly ...*mmmmrrmmmm*... stereoerrors in the isotactoid sequences and of ...*rrrrmrrrr*... stereoerrors in the syndiotactic ones) are reproduced, on the other hand the fit is far from being satisfactory, as the unacceptably high value of the reduced χ^2 function ($\chi_r^2 = 15.9$) indicates.

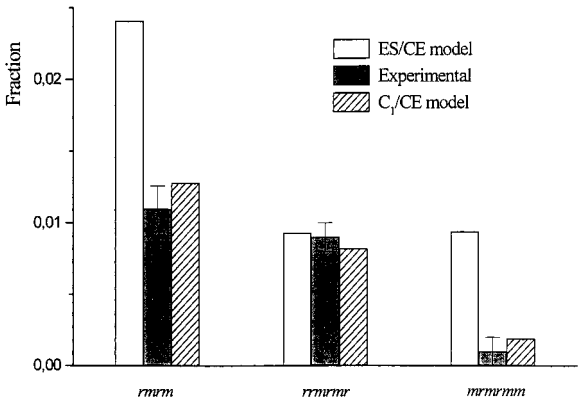

Figure 2. Comparison between experimental fractions of the *rmrm*-centered *n*ads in fraction A and best-fit calculated ones in terms of the ES/CE and C_1/CE models (see text).

The fact that the model is still considered to be adequate at the pentad level is not contradictory. To our knowledge, very few attempts of estimating the experimental error on polypropylene pentad distributions determined by "routine" ^{13}C NMR have been reported in the literature;[17] in most cases, however, the fractional abundances of the various pentads are serendipitously expressed with two decimal digits.[13,14] If it is admitted that the uncertainty is (at least) ± 1 on the last digit, it is easy to verify that, once applied to such data, the ES/CE model results in χ_r^2 values not far from 1 and that more complex models, necessarily requiring a higher number of adjustable parameters, lead to overfitting.

Improving the Two-Site Model: the C_1/CE Model. When comparing the two distributions in columns 3 and 4 of Table 1, it can be noted that the largest disagreement (in relative sense) affects the $m_x rmrm_y$ *n*ads (e.g., *mrmrm* and *mmrmr* hexads, *mmmrmr* and *mrmrmm* heptads), whose calculated fractions are much larger than the experimental ones. The case of the *rmrm*-centered sequences can be used as an exemplification (see also Figure 2): the fractional abundance of the *rmrm* pentad calculated according to the ES/CE model is more than twice the experimental one, and the reason for that is a 10-fold overestimate of the *mrmrmm* heptad (whereas the *rrmrmr* heptad, mostly occurring in syndiotactic sequences, is correctly reproduced).

$m_x rmrm_y$ *n*Ads should derive from isotactoid sequences containing two consecutive stereoerrors (Chart 1a).

According to the enantiomorphic sites statistics,[4] all *n*ads of equal length and equal number of stereoirregular units are equiprobable. This is clearly not the case for the investigated sample, in which only *n*ads with nonconsecutive stereoerrors (such as, e.g., *mrrmmrrm* and *mmrrmr*, Chart 1b,c) were detected.

In ref 1d, we noted that this feature is typical of predominantly isotactic polypropylenes prepared with homogeneous catalysts based on C_1-symmetric *ansa*-metallocenes of the fourth column of the type sketched in Chart 2a (with X a bulky group such as, e.g., *tert*-butyl or trimethylsilyl)[18] or Chart 2b,[19] with two diastereotopic[20] active sites (denoted in the charts as 1 and 2).

For such catalysts, it is generally accepted that the polymerization proceeds with a "defective chain migratory" mechanism.[18,19,21] Indeed, molecular mechanics calculations[21] pointed out a preference of the growing chain for the sterically more open coordination site 2;

Chart 1

Chart 2

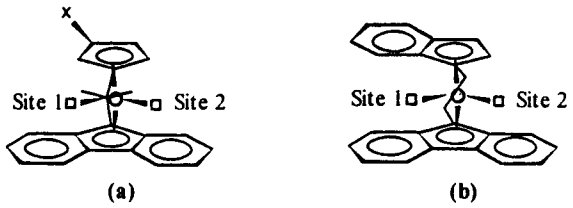

as a result, monomer insertion occurs preferentially at site 1. The fact that only site 1 is highly enantioselective[21] has the following consequences: (i) Chain propagation is predominantly isotactic. (ii) The stereoselectivity increases with decreasing monomer concentration, because this favors chain "back-skip" relative to monomer insertion at the weakly enantioselective site 2. (iii) The probability of two consecutive insertions at site 2 (and hence that of two consecutive stereoerrors) is very low, which means that sequences of the type $m_x r m r m_y$ are virtually "prohibited".

Importantly, an inverse correlation between stereoselectivity and monomer concentration holds also for the active species of the heterogeneous Ziegler−Natta systems responsible for the formation of the isotactoid sequences.[1d] This finding, along with the discussed selection rule of stereosequence generation, suggests a close similarity with the case of the quoted[18,19,21] C_1-symmetric metallocenes.

Therefore, we replaced matrix **E** of the ES/CE model with a more general one, apt to describe site-controlled chain propagation at a C_1-symmetric active species with two diastereotopic sites:

$\boldsymbol{C_1}$ =

	R	S	R	S
R	$\sigma_1(1-P_{12})$	$(1-\sigma_1)(1-P_{12})$	$\sigma_2 P_{12}$	$(1-\sigma_2)P_{12}$
S	$\sigma_1(1-P_{12})$	$(1-\sigma_1)(1-P_{12})$	$\sigma_2 P_{12}$	$(1-\sigma_2)P_{12}$
R	$\sigma_1 P_{21}$	$(1-\sigma_1)P_{21}$	$\sigma_2(1-P_{21})$	$(1-\sigma_2)(1-P_{21})$
S	$\sigma_1 P_{21}$	$(1-\sigma_1)P_{21}$	$\sigma_2(1-P_{21})$	$(1-\sigma_2)(1-P_{21})$

σ_1 and σ_2 are the conditional probabilities that the prochiral monomer inserts with a given enantioface (either *re* or *si*) at each of the two sites (1 and 2, respectively), as a result of site chirotopicity;[20] P_{12} and P_{21} are the conditional probabilities of monomer insertion at site 2 after a previous insertion at site 1 and vice versa. Ideal chain migratory propagation requires that $P_{12} = P_{21} = 1$; in this case, $\sigma_1 \approx 1$ (or ≈ 0) and $\sigma_2 \approx 0.5$ corresponds to hemiisotactic propagation.[22]

From here on, we will refer to this as the "C_1 model". A linear combination with the CE model results in a C_1/CE two-site model with six adjustable parameters (σ_1, σ_2, P_{12}, P_{21}, P_r, w_{C_1}).

In column 5 of Table 1, we report the best-fit stereosequence distribution for fraction A. The absolute minimum corresponds to $\chi_r^2 = 5.6$, which is indicative of a substantial improvement of the fit compared with the ES/CE model; in particular, the experimental fractions of most $m_x r m r m_y$ nads are now nicely matched (see again Figure 2).

The best-fit values of P_r (=0.89) and of the mixing coefficient (=0.47) are identical to those found for the ES/CE model, and the differences concern entirely isotactoid propagation. According to the C_1/CE model, this takes place at an active species inserting the monomer predominantly at a highly enantioselective site (site 1: $\sigma_1 \approx 0.99$, $P_{12} < P_{21}$), and the probability $(1 - P_{21})$ of two consecutive insertions at the other site, of much lower enantioselectivity (site 2: $\sigma_2 \approx 0.6$), is practically 0. The analogy with the metallocene case is obvious.

The minimum of the χ_r^2 function, however, is rather shallow, and acceptable values of χ_r^2 are obtained for all solutions in which $P_{12}(1 - \sigma_2)$ (i.e., the fraction of stereoerrors in the isotactoid sequences) is ≈ 0.2 and $0.3 < \sigma_2 < 0.7$.

It might be noted at this point that an alternative way of reproducing the experimental absence of consecutive stereoerrors in the isotactoid sequences would be to perturb the ES statistics by admitting that the stereocontrol exerted by the chirality of the active metal centers is influenced by the asymmetry of the last-inserted monomeric unit and that in the resulting first-order Markovian distribution of *configurations* the following scheme of conditional probabilities holds:

$$P_{XX} \gg P_{XY}; \quad P_{YY} \approx 0$$

(with X = R or S and Y = S or R).

A model of this kind has been recently illustrated by Randall,[8] who stressed the possibility of ambiguities in the statistical analysis of polymer microstructure by recalling Price's observation[23] that "Markovian mathematics .... is only a framework within which it is possible to describe polymer chains having particular sequential characteristics, regardless of how these chains were produced".

This statement is correct when applied to cases in which the microstructural data represent the only available experimental information. In the case under investigation, however, the independent observation[1d] that the stereoregularity of the isotactoid sequences increases with decreasing monomer concentration finds an immediate and simple explanation within the C_1 statistics, in terms of a corresponding increase of the frequency of chain back-skip $(1 - P_{12})$ compared with that of monomer insertion at site 2. Therefore, we can assume the C_1/CE model as a sound basis for further improvements.

To this end, let us examine the residual mismatches between experimental and best-fit stereosequence distribution (columns 3 and 5 of Table 1). These concern mainly the *mmmmmr*, *mmmmrr*, and *mmrrmm* heptads, which are overestimated in the calculations, and the *rrrrmm*, *rmrrmr*, and *mmrrmr* heptads, which are instead largely underestimated (Chart 3 and Figure 3).

Altogether, these observations clearly indicate that the stereoerrors in the predominantly isotactic sequences have a "blocky" distribution. The copresence of "less defective" and "more defective" isotactic blocks, in addition to the syndiotactic ones, calls for the adoption of a three-site model.

Chart 3

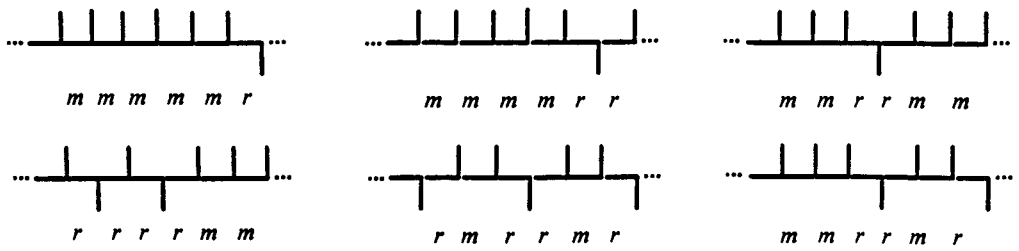

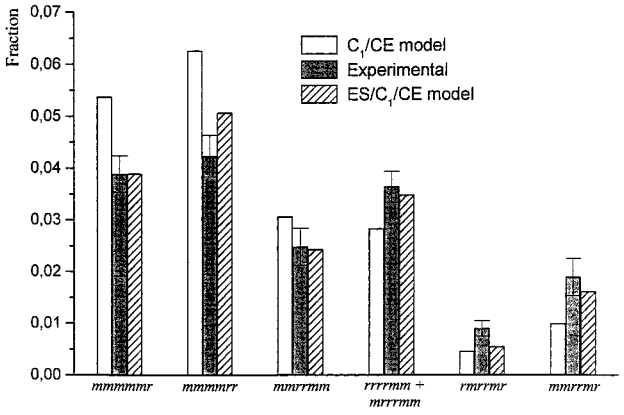

Figure 3. Comparison between experimental fractions of selected *n*ads of fraction A and best-fit calculated ones in terms of the C_1/CE and ES/C_1/CE models (see text).

The ES/C_1/CE Three-Site Model. Three-site models for describing the configurational statistics of polypropylenes made with Ziegler−Natta catalysts have already been proposed.[6,7,14d] However, due to the high number of adjustable parameters (≥5), their application to "routine" ^{13}C NMR data at the pentad level should be regarded as unfeasible.

In our case, the availability of high-resolution ^{13}C NMR data made it possible to use three-site models in a statistically significant manner for the first time.

A general C_1/C_1/CE model, with as many as 11 adjustable parameters (four for each $\boldsymbol{C_1}$ matrix, one for the **C** matrix, and two mixing coefficients), appeared unreasonably complicated even for the expanded set of microstructural data in Table 1. On the other hand, due to the fact that the ES and C_1 statistics tend to degenerate with increasing stereoselectivity of chain propagation,[1d] the former was tentatively adopted for describing the configuration of the "less defective" isotactic sequences. This resulted in a more simple ES/C_1/CE model with eight adjustable parameters (σ for ES propagation; σ_1, σ_2, P_{12}, P_{21} for C_1 propagation; P_r for CE propagation; the two mixing coefficients w_{ES} and w_{C_1}).

The best-fit stereosequence distribution for fraction A in terms of such a model is given in the sixth column of Table 1. At the absolute minimum, χ_r^2 is now as low as 1.46 (close to the "ideal" value of $\chi_r^2 = 1$), and most $|(y_{i,c} - y_{i,o})|$ values are actually lower than the experimental uncertainties (see also Figure 3).

According to the model, the investigated polypropylene fraction consists of *three* different types of stereosequences: highly isotactic, isotactoid, and syndiotactic. The former, in low amount (≈10 wt %), would be close to ideal isotacticity, with less than 1 mol % of isolated stereoirregular units. The isotactoid sequences would amount to ≈40 wt % and contain ≈30 mol % of stereoirregular units, distributed in accordance with the C_1 statistics. The remaining ≈50 wt % of the material would be formed by syndiotactic sequences, with ≈10 mol % of stereoirregular units consistent with chain-end control.

Also in this case, however, as already discussed in the previous section, the χ_r^2 function is almost invariant for all solutions in which $P_{12}(1 - \sigma_2)$ is ≈0.3. This leaves a substantial uncertainty on the actual value of σ_2; indeed, similar distributions of configurations can be achieved in all cases comprised between the following two limiting hypotheses: (i) site 1 is highly enantioselective ($\sigma_1 \approx 1$), whereas site 2 is nonenantioselective ($\sigma_2 \approx 0.5$); (ii) sites 1 and 2 are enantiotopic and both highly enantioselective ($\sigma_1 \approx 1$, $\sigma_2 \approx 0$ or $\sigma_1 \approx 0$, $\sigma_2 \approx 1$).

In our opinion, it is particularly worthy of note that the value of σ in the **E** matrix and of σ_1 in the $\mathbf{C_1}$ matrix are very similar (and close to 1). Moving from this observation, it is tempting to formulate the hypothesis that the highly isotactic sequences are formed at catalytic species with one or two active sites identical to site 1 of the C_1-symmetric species producing the isotactoid sequences but differing from the latter in that the "error-generating" site (site 2) is either missing or not accessible. The above can be translated in the following constraint

$$\sigma = \sigma_1$$

and results in a simplified version of the ES/C_1/CE model, with "only" seven adjustable parameters (σ_1, σ_2, P_{12}, P_{21}, P_r, w_{ES}, w_{C_1}).

When applied to the experimental data of Table 1, this version gave a best-fit (last column of the same table) with $\chi_r^2 = 1.40$ (that is, slightly less than for the more general version).

Configurational Analysis of the "Isotactic" Fraction B. Due to the higher stereoregularity of fraction B compared with that of fraction A, the experimental conditions for the ^{13}C NMR characterization had to be varied.

In the first place, an acquisition temperature as high as 130 °C was needed for complete sample dissolution. Of course, appreciable variations of the chemical shift values relative to the reference polypropylene spectra at 70 °C reported in ref 2 were observed. To avoid ambiguities, the resonance assignment was checked by comparison with the same reference spectra rerecorded at 130 °C.

In the second place, the lower fraction of "defective" stereosequences resulted in a less crowded spectrum, with strong multiplets corresponding to m_n *n*ads (n = 5−7) and a number of much weaker resonances. On one hand, this allowed to achieve an adequate resolution already at 125 MHz. On the other hand, it required a more concentrated polymer solution in order to reach

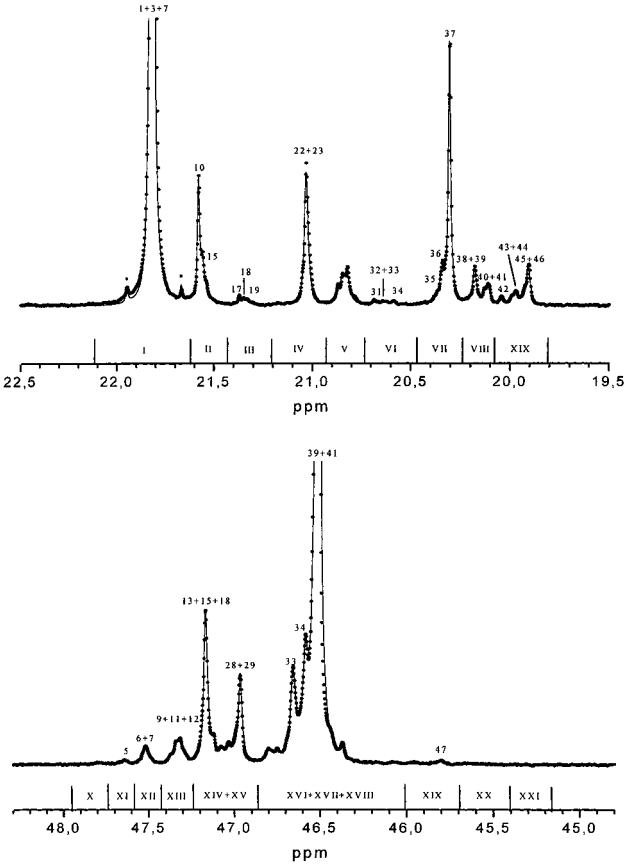

Figure 4. Experimental (dotted) and simulated (solid) 125 MHz ^{13}C NMR spectrum of fraction B (in tetrachloroethane-*1,2-d*$_2$ solution at 130 °C). The δ scale is in ppm downfield of TMS; peak and range numbering refers to the full assignment reported in ref 2. $^{13}C-^{13}C$ satellite peaks are starred. (a, top) Methyl region; (b, bottom) methylene region.

the high signal-to-noise ratio needed for a reliable integration in a reasonable experiment time; as a consequence, the peaks were slightly broadened by entangling effects.

The 125 MHz ^{13}C NMR spectrum of fraction B at 130 °C is shown in Figure 4 (peak numbering refers to the full assignment given in ref 2). By comparison with the spectrum of fraction A at 70 °C (Figure 1), it is easy to realize that the higher temperature determined a significant shrinkage of the chemical shift spreading; as a matter of fact, only the methyl region and some parts of the methylene region could be used for quantitative measurements of stereosequence distribution. This notwithstanding, a set of 23 independent data, ranging from pentads to nonads, could be obtained (Table 2).

Due to the limitations discussed above, the complex least-squares fit of the spectrum as a summation of Lorentzian peaks[15] (also shown in Figure 4) turned out to be of comparatively poor quality. Therefore, peak areas were evaluated from numerical integrals, the fit being used only to correct the latter for the unavoidable improper cutting of the long Lorentzian tails.[15b]

In the same Table 2, we report the best-fit distributions calculated according to the ES/CE two-site model and to the ES/C_1/CE three-site model.

Also in this second case, the ES/CE model was found not to be adequate ($\chi_r^2 = 7.1$). Even worse results were obtained for the ES/C_1 model ($\chi_r^2 = 8.4$; data not reported).

Conversely, the application of the ES/C_1/CE model resulted in a very good match between experimental and calculated data, with absolute minimum values of χ_r^2 of 2.2 both for the eight-parameter version (data not reported) and for the seven-parameter version. Once more, we found that acceptable values of χ_r^2 are obtained for all solutions in which the product $P_{12}(1 - \sigma_2)$ (that is, the fraction of stereoerrors in the isotactoid sequences) is $\approx$0.2 and $0 < \sigma_2 < 0.5$ (with corresponding adjustments of the other parameters).

Strikingly, the best-fit values of the conditional probabilities σ_1 and P_r turned out to be identical (within the experimental uncertainty) to those for fraction A (cf. Table 1). As a matter of fact, the main difference between the two fractions consists in the relative amounts of the three types of constituting stereosequences (for fraction B: 55 $\pm$ 10% highly isotactic, 35 $\pm$ 10% isotactoid, and 15% syndiotactic).

Comparison with Literature Interpretations of "Low-Resolution" ^{13}C NMR Microstructural Data. In a previous section, we have already recalled that an ES/ES/CE three-site model for reproducing the methyl pentad distributions of polypropylene samples made with Ziegler–Natta catalysts was proposed by Cheng 10 years ago,[6] in a constrained form that provides a microstructural description conceptually similar to the one we have derived with our ES/C_1/CE model; indeed, the enantioselectivity of each of the two ES sites was forced to be the same for heptane-insoluble and heptane-soluble fractions.

More recently, a general ES/ES/CE model was applied to propene polymerization promoted by $MgCl_2$-supported catalysts by van der Burg et al.[7] and by Paukkeri et al.[14d] Interestingly, the latter authors noted the tendency of the calculations to overestimate the *rmrm* pentad (as a whole), as well as the decrease of the isotactic selectivity with increasing monomer concentration, but did not correlate the two observations.

On the other hand, we stress once again that using *any* three-site model for the statistical analysis of polypropylene microstructure at the "routine" pentad level invariably leads to overfitting. In this respect, Cheng's proposal[6] should be regarded as a clever intuition; as a matter of fact, we found that, due to the deviation of the stereosequence distribution in the isotactoid sequences from the enantiomorphic sites statistics, when applied to the high-resolution ^{13}C NMR data of Tables 1 and 2, the ES/ES/CE model reduces to an ES/CE model in the case of fraction A, whereas in that of fraction B it ends up with a χ_r^2 value of 7.2.

Correlations between Microstructure and Physical Properties of the Materials. According to our interpretation of the high-resolution ^{13}C NMR data, the investigated "atactic" and "isotactic" polypropylene fractions comprise the same three building blocks (the configuration of the highly isotactic, isotactoid, and syndiotactic sequences being almost invariant) and differ merely in their relative amounts.

This conclusion necessarily implies their stereoblock nature. Indeed, the fact that fraction A is soluble in boiling pentane indicates that the highly isotactic sequences are relatively short; conversely, the only explanation for the presence of isotactoid sequences in the xylene-insoluble fraction B is that they are chemically bound to crystalline highly isotactic and/or syndiotactic sequences.

Table 2. Stereosequence Distribution of Fraction B (for the Definition of the Adjustable Parameters, See Text)

		normalized fraction				
range/peak no.	assignt	exptl	calcd, ES/CE		calcd, ES/C_1/CE (constrained)	
I	*mmmm*	0.6515(18)	0.6530		0.6524	
II	*mmmr*	0.0621(12)	0.0635		0.0591	
III	*rmmr*	0.0065(5)	0.0036		0.0065	
III/17	*mrrmmrrm*	0.0025 (7)	0.0013		0.0034	
III/18	*mrrmmrrr*	0.0019(9)	0.0005		0.0015	
IV	*mmrr*	0.0670(8)	0.0669		0.0685	
V	*mmrm* + *rmrr*	0.0378(13)	0.0357	0.0037 0.0320	0.0358	0.0037 0.0321
VI	*rmrm*	0.0060(5)	0.0072		0.0063	
VI/31	*rrmrmr*	0.0020(10)	0.0032		0.0022	
VI/34	*mrmrmm*	0.0020(10)	0.0028		0.0026	
VII	*rrrr*	0.1045(7)	0.1046		0.1046	
VIII/38+39	*mrrrmr*+ *rrrrmr*	0.0180(14)	0.0255	0.0032 0.0223	0.0202	0.0023 0.0179
VIII/40+41	*rrrrmm* + *mrrrmm*	0.0130(20)	0.0064	0.0058 0.0006	0.0129	0.0122 0.0007
IX	*mrrm*	0.0341(8)	0.0335		0.0337	
IX/43+44	*mmrrmr*	0.0129(33)	0.0032		0.0087	
IX/45+46	*mmrrmm*	0.0192(17)	0.0287		0.0234	
X	*mrmrm*	0.0013(8)	0.0017		0.0016	
XI	*mrmrr*	0.0028(13)	0.0038		0.0030	
XII	*rrmrr* + *mrrrm*	0.0149(15)	0.0160	0.0141 0.0019	0.0161	0.0146 0.0015
XIII	*mrrrr*	0.0274(36)	0.0282		0.0301	
XIV+ XV	*rmmrm* + *rrrrr* + *rmmrr* + *mmmrm* + *mmmrr*	0.1571(103)	0.1612	0.0008 0.0905 0.0064 0.0030 0.0605	0.1617	0.0008 0.0896 0.0122 0.0028 0.0563
XIX	*rmrmr*	0.0042(17)	0.0019		0.0015	
XX	*mmrmr*	0.0010(10)	0.0034		0.0033	
			$\Sigma(y_{i,c}-y_{i,o})^2 \times 10^4 = 3.39$, $\chi_r^2 = 7.1$		$\Sigma(y_{i,c}-y_{i,o})^2 \times 10^4 = 1.01$, $\chi_r^2 = 2.2$	
			$\sigma = 0.95$			
					$\sigma_1 = 0.99_8$ $\sigma_2 = 0.39$ $P_{12} = 0.28$ $P_{21} = 0.92$ $P_r = 0.91$ $w_{ES} = 0.51$ $w_{C_1} = 0.35$	
			$P_r = 0.88$ $w_{ES} = 0.83$			

Unfortunately, in the investigated cases, the detection of the chemical junctions is beyond the possibilities of the microstructural analysis even when high-resolution ^{13}C NMR is used. As a result, nothing can be said about the sequence of the three types of stereoblocks within the individual macromolecules.

Despite this limitation, our model fits nicely with the observed physical properties of the materials. In particular, on one hand, it provides a simple explanation for the fact that fraction B, with an *average* content of stereoirregularities in the isotactic part of almost 5 mol %, has a DSC melting peak with the maximum at 157 °C (Figure 5), whereas polypropylene samples with the same amount of *uniformly distributed* defects, made with "single-site" metallocene catalysts, melt around 130 °C.[24]

On the other hand, it easily accounts for the (otherwise surprising) observation of weak isotactic crystallinity in the X-ray diffraction spectrum of fraction A as well (Figure 6). In fact, this can be traced to the low amounts of highly isotactic blocks rather than to an improbable large compatibility of the stereoerrors in the isotactoid blocks with the crystal lattice.

Implications of the Microstructural Results on the Nature of the Catalytic Species. This investigation has provided sound experimental evidence that the isotactoid sequences are formed at C_1-symmetric surface Ti complexes with two diastereotopic active sites; monomer insertion would occur preferentially at one of such sites, of very high enantioselectivity, but the insertion frequency at the other site would be nonnegligible and mostly result in the formation of stereoirregularities.

We can plausibly imagine that the relative insertion rates are determined by nonbonded interactions of the monomer and/or of the growing chain with the ligand

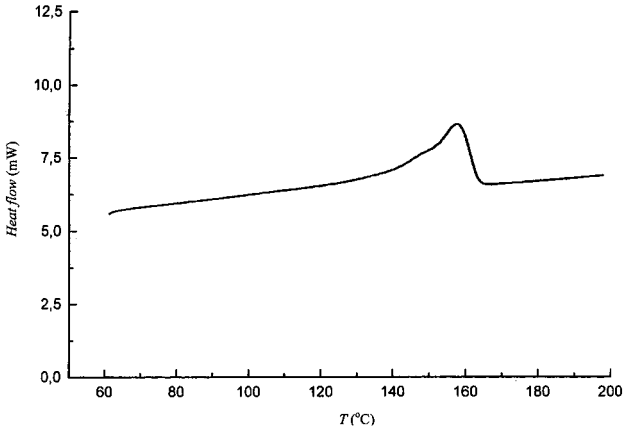

Figure 5. DSC heating curve of fraction B.

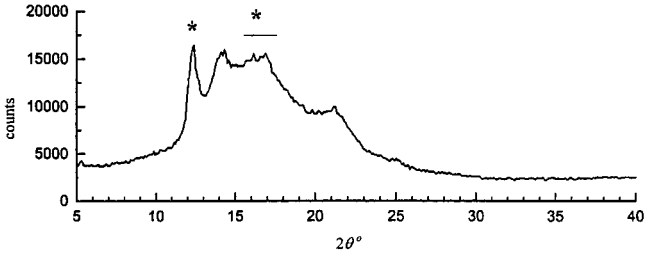

Figure 6. X-ray powder diffraction spectrum of fraction A. Regions including reflections due to syndiotactic crystallinity are marked with asterisks.

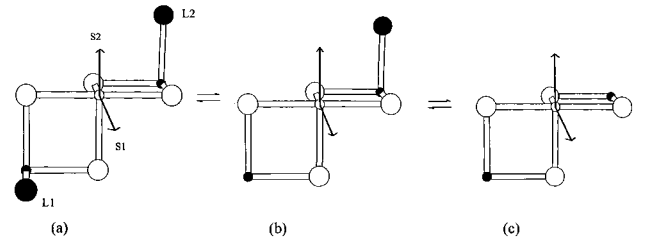

Figure 7. Possible models of active species for highly isotactic (a), isotactoid (b) and syndiotactic propagation (c) (see text). ○ = Ti; ● = Ti or Mg; ○ = Cl; ● = Cl or donor.

environment of the transition metal.[11] If we accept that the basic structure of the catalytic complex is that proposed long ago by Cossee and Arlman[25] and elaborated by Corradini and co-workers[26] (Figure 7), we note that differences in the substitution of the two coordination positions labeled in the figure as L1 and L2, known to be crucial for the onset of site control in terms of the "growing-chain orientation mechanism",[11,26] can provide a simple and unifying explanation for the observed chain propagation mechanisms.

In particular:

(i) Isotactoid propagation can correspond to having a ligand (e.g., a Cl atom, an Al−alkyl, or a Lewis base molecule) in only one of such two coordination positions (C_1 symmetry).

(ii) Highly isotactic propagation can correspond to having ligands in both positions (C_2 or pseudo-C_2 symmetry with homotopic active sites), or only one ligand with a steric hindrance high enough to inhibit monomer insertion at the "error-generating" site (S2 in the figure).

(iii) Syndiotactic propagation can correspond to having both coordination positions vacant, so that site control is lost and chain-end control can become influent.

(iv) Ligand exchanges at positions L1 and L2 can be the reason for reversible switches between the different types of stereocontrol, with the resulting formation of stereoblock chains.

(v) "Second-order" effects (such as, in particular, the conditional probability of monomer insertion at the "error-generating" site of the C_1-symmetric species, and therefore the average content of stereoirregularities in the isotactoid sequences) might be related to the specific nature of the ligand(s) involved.

Models of active sites that might fit, in part, with these considerations have been recently proposed by Scordamaglia and Barino.[27]

Conclusions

The stereosequence distribution of the "atactic" and "isotactic" fractions of a polypropylene sample made with a $MgCl_2$-supported catalyst was determined by means of high-resolution ^{13}C NMR[1,2] and analyzed in terms of statistical models of increasing sophistication.

Two-site models, including the one normally used for the interpretation of "routine" ^{13}C NMR data at the pentad level,[5] were shown to be inconsistent with the much finer high-resolution data. A good agreement between experimental and calculated stereosequence distributions could be obtained only in terms of a three-site model, describing each fraction as a mixture of highly isotactic, weakly isotactic ("isotactoid") and syndiotactic sequences. According to such a model, the two fractions comprise the same three building blocks (the configuration of the three different types of stereosequences being almost invariant) and differ merely in their relative amounts; this conclusion necessarily implies a stereoblock nature.

This interpretation provides a simple and logical explanation for the observed physical properties of the materials (and in particular for their crystallization behavior).

It also represents a starting point for the development of better defined models of the active species in $MgCl_2$-supported Ziegler−Natta catalysts.

Both aspects will be addressed in more detail in separate papers.

Experimental Part

Preparation and Fractionation of the Polypropylene Sample. The synthesis was carried out in a 1 L stainless steel reactor (Brignole AU-1) equipped with a magnetic stirrer (1000 rpm) and a catalyst vial holder/breaker. A solution of $Al(C_2H_5)_3$ (Witco, 4.2 mmol) and 2,6-dimethylpyridine (Aldrich, 1.7 mmol) in anhydrous heptane (300 mL) was charged in the reactor, thermostated at 60 °C, and saturated with propene at the partial pressure of 2.5 bar. The reaction was started by breaking a glass vial containing 100 mg of a $MgCl_2/TiCl_4$ catalyst (Ti content, 2.0 wt %),[12b,c] sealed under argon in a Vacuum Atmospheres glovebox, allowed to proceed at constant monomer pressure for 30 min, and stopped by monomer degassing. The polymer was coagulated with methanol (1 L), filtered, and vacuum-dried.

Fraction A (diethyl ether-insoluble/pentane-soluble) was isolated by exhaustive Kumagawa extraction with boiling diethyl ether and pentane in sequence. Fraction B (xylene-insoluble) was obtained by fractional crystallization after dissolution in xylene.[12k,13g]

^{13}C NMR Characterizations. The $^{13}C\{^1H\}$ NMR spectrum of fraction A (Figure 1) was recorded with a Bruker AMX 600 spectrometer operating at 150.9 MHz, on a 5 mg/mL polymer solution in tetrachloroethane-*1,2-d*$_2$ at 70 °C. Experimental setup: acquisition time, 2.3 s; relaxation delay, 2.0 s; pulse angle, 45°; 64K data points; 25K transients. Proton broad-band decoupling was achieved with the GARP sequence.[28] The $^{13}C\{^1H\}$ NMR spectrum of fraction B (Figure 4) was recorded with a Bruker DRX 500 spectrometer operating at 125.76 MHz, on a 150 mg/mL polymer solution in tetrachloroethane-*1,2-d*$_2$ at 130 °C. Experimental setup: acquisition time, 3.25 s; relaxation delay, 1.0 s; pulse angle, 90°; 64K data points; 16.7K transients. Proton broad-band decoupling was achieved with the WALTZ16 sequence.[29] In both cases, a probe for 5 mm tubes was used.

After zero filling, Fourier transformation was performed either without any further correction or—for resonance assignment only—after the application of a weak resolution-enhancing Gaussian function. Baseline corrections and peak integrations were performed with the "SHAPE" program.[15b] All best-fit calculations of stereosequence distribution were carried out with the "CONFSTAT" program.[16]

Other Characterizations. Intrinsic viscosities were measured in tetralin at 135 °C, with a standard Ubbelohde

viscometer ($K = 1.93 \times 10^{-4}$, $\alpha = 0.74$). DSC curves were recorded with a Perkin-Elmer DSC-7 calorimeter, at a scanning rate of 10 K/min. X-ray diffraction spectra were collected from compression-molded plates with a Philips PW 2273/20 automatic powder diffractometer, using Ni-filtered Cu Kα radiation.

References and Notes

(1) (a) Busico, V.; Corradini, P.; De Biasio, R.; Landriani, L.; Segre, A. L. *Macromolecules* **1994**, *27*, 4521. (b) Corradini, P.; Busico, V.; Cipullo, R. *Catalyst Design for Tailor-Made Polyolefins*; Soga, K., Terano, M., Eds.; Kodansha: Tokyo, 1994; pp 21−34. (c) Busico, V.; Cipullo, R.; Corradini, P.; Landriani, L.; Vacatello, M.; Segre, A. L. *Macromolecules* **1995**, *28*, 1887. (d) Busico, V.; Cipullo, R.; Talarico, G.; Segre, A. L.; Chadwick, J. C. *Macromolecules* **1997**, *30*, 4787. (e) Busico, V. *Proceedings of the International Symposium on Metallorganic Catalysts for Synthesis and Polymerization*, Hamburg, Sept 13−17, 1998.

(2) (a) Busico, V.; Cipullo, R.; Monaco, G.; Vacatello, M.; Segre, A. L. *Macromolecules* **1997**, *30*, 6251. (b) Busico, V.; Cipullo, R.; Monaco, G.; Vacatello, M.; Bella, J.; Segre, A. L. *Macromolecules* **1998**, *31*, 8713.

(3) Bovey, F. A.; Tiers, G. V. D. *J. Polym. Sci.* **1960**, *44*, 173.

(4) Shelden, R. A.; Fueno, T.; Tsunetsugu, T.; Furukawa, J. *J. Polym. Sci., Polym. Lett.* **1965**, *3*, 23.

(5) Doi, Y. *Makromol. Chem., Rapid Commun.* **1982**, *3*, 635.

(6) Cheng, H. N. *J. Appl. Polym. Sci.* **1988**, *35*, 1639.

(7) van der Burg, M.; Chadwick, J. C.; Sudmeijer, O.; Tulleken, H. J. A. F. *Makromol. Chem., Theory Simul.* **1993**, *2*, 399.

(8) Randall, J. C. *Macromolecules* **1997**, *30*, 803.

(9) Boor, J. *Ziegler−Natta Catalysts and Polymerizations*; Academic Press: New York, 1979.

(10) Kissin, Y. V. *Isospecific Polymerization of Olefins*; Springer-Verlag: New York, 1985.

(11) Corradini, P.; Busico, V.; Guerra, G. In *Comprehensive Polymer Science*; Pergamon Press: Oxford, 1988; Vol. 4, pp 29−50.

(12) Experimental studies of propene polymerization promoted by $MgCl_2$-supported catalysts: (a) Galli, P.; Luciani, L.; Cecchin, G. *Angew. Makromol. Chem.* **1981**, *94*, 63. (b) Busico, V.; Corradini, P.; De Martino, L.; Proto, A.; Savino, V.; Albizzati, E. *Makromol. Chem.* **1985**, *186*, 1279. (c) Busico, V.; Corradini, P.; De Martino, L.; Proto, A.; Albizzati, E. *Makromol. Chem.* **1986**, *187*, 1115. (d) Barbè, P. C.; Cecchin, G.; Noristi, L. *Adv. Polym. Sci.* **1987**, *81*, 1. (e) Soga, K.; Shiono, T.; Doi, Y. *Makromol. Chem.* **1988**, *189*, 1531. (f) Proto, A.; Oliva, L.; Pellecchia, C.; Sivak, A. J.; Cullo, L. A. *Macromolecules* **1990**, *23*, 2904. (g) Noristi, L.; Barbè, P. C.; Baruzzi, G. *Makromol. Chem.* **1991**, *192*, 1115. (h) Noristi, L.; Barbè, P. C.; Baruzzi, G. *Makromol. Chem.* **1992**, *193*, 229. (i) Kioka, M.; Makio, H.; Mizuno, A.; Kashiwa, N. *Polymer* **1994**, *35*, 580. (j) Albizzati, E.; Giannini, U.; Morini, G.; Galimberti, M.; Barino, L.; Scordamaglia, R. *Macromol. Symp.* **1995**, *89*, 73. (k) Chadwick, J. C.; Morini, G.; Albizzati, E.; Balbontin, G.; Mingozzi, I.; Cristofori, A.; Sudmeijer, O.; van Kessel, G. M. M. *Macromol. Chem. Phys.* **1996**, *197*, 2501.

(13) ^{13}C NMR microstructural characterizations at the pentad level of polypropylene fractions obtained by extraction with boiling solvents or crystallization from xylene solutions: (a) Wolfsgruber, C.; Zannoni, G.; Rigamonti, E.; Zambelli, A. *Makromol. Chem.* **1975**, *176*, 2765. (b) Zhu, S.-N.; Yang, X.-Z.; Chûjô, R. *Polym. J.* **1983**, *12*, 859. (c) Inoue, Y.; Itabashi, Y.; Chûjô, R.; Doi, Y. *Polymer* **1984**, *25*, 1640. (d) Martuscelli, E.; Avella, M.; Segre, A. L.; Rossi, E.; Di Drusco, G.; Galli, P.; Simonazzi, T. *Polymer* **1985**, *26*, 259. (e) Hayashi, T.; Inoue, Y.; Chûjô, R.; Doi, Y. *Polymer* **1989**, *30*, 1714. (f) Busico, V.; Corradini, P.; De Martino, L.; Graziano, F.; Iadicicco, A. *Makromol. Chem.* **1991**, *192*, 49 (g) Chadwick, J. C.; Miedema, A.; Ruisch, B. J.; Sudmeijer, O. *Makromol. Chem.* **1992**, *193*, 1463. (h) Busico, V.; Cipullo, R.; Corradini, P.; De Biasio, R. *Macromol. Chem. Phys.* **1995**, *196*, 491.

(14) ^{13}C NMR microstructural characterizations at the pentad level of polypropylene fractions obtained by temperature rising elution fractionation: (a) Pavan, A.; Provasoli, A.; Moraglio, G.; Zambelli, A. *Makromol. Chem.* **1977**, *178*, 1099. (b) Kakugo, M.; Miyatake, T.; Naito, Y.; Mizunuma, K. *Macromolecules* **1988**, *21*, 314. (c) Paukkeri, R.; Väänänen, T.; Lehtinen, A. *Polymer* **1993**, *34*, 2488. (d) Paukkeri, R.; Iiskola, E.; Lehtinen, A.; Salminen, H. *Polymer* **1994**, *35*, 2636. (e) Härkönen, M.; Seppälä, J. V.; Salminen, H. *Polym. J.* **1995**, *27*, 256.

(15) (a) Martin, Y.-L. *J. Magn. Reson. A* **1984**, *111*, 1. (b) Simulation performed with the "SHAPE" program by: Monaco, G., University of Naples "Federico II". Monaco, G., manuscript in preparation.

(16) "CONFSTAT" program: Vacatello, M. University of Naples "Federico II"; see also refs 1c and 2.

(17) van der Burg, M.; Chadwick, J. C.; Sudmeijer, O.; Tulleken, H. J. A. F. *Makromol. Chem., Theory Simul.* **1993**, *2*, 385.

(18) (a) Ewen, J. A.; Elder, M. J. Eur. Pat. Appl. 537130, 1993. (b) Ewen, J. A. *Macromol. Symp.* **1995**, *89*, 181 and references therein. (c) Razavi, A.; Peters, L.; Nafpliotis, L.; Verecke, D.; Den Dauw, K.; Atwood, J. L.; Tewald, U. *Macromol. Symp.* **1995**, *89*, 345 and references therein.

(19) Rieger, B.; Jany, G.; Fawzi, R.; Steinmann, M. *Organometallics* **1994**, *13*, 647.

(20) Farina, M. *Macromol. Symp.* **1995**, *89*, 489.

(21) Guerra, G.; Cavallo, L.; Moscardi, G.; Vacatello, M.; Corradini, P. *Macromolecules* **1996**, *29*, 4834.

(22) (a) Farina, M.; Di Silvestro, G.; Sozzani, P.; Savaré, B. *Macromolecules* **1985**, *18*, 923. (b) Farina, M.; Di Silvestro, G.; Sozzani, P.; Savaré, B. *Macromolecules* **1985**, *18*, 928. (c) Farina, M.; Di Silvestro, G.; Sozzani, P. *Macromolecules* **1993**, *26*, 946.

(23) Price, F. P. In *Markov Chains and Monte Carlo Calculations in Polymer Chains*; Lowry, G. G., Ed.; Marcel Dekker: New York, 1970; Chapter 7.

(24) Unpublished results of our laboratory. See also: Fischer, D.; Mülhaupt, R. *Macromol. Chem. Phys.* **1994**, *195*, 1433.

(25) (a) Corradini, P.; Barone, V.; Fusco, R.; Guerra, G. *Eur. Polym. J.* **1979**, *15*, 1133. (b) Corradini, P.; Guerra, G.; Fusco, R.; Barone, V. *Eur. Polym. J.* **1980**, *16*, 835. (c) Corradini, P.; Barone, V.; Fusco, R.; Guerra, G. *J. Catal.* **1982**, *77*, 32. (d) Corradini, P.; Barone, V.; Fusco, R.; Guerra, G. *Gazz. Chim. Ital.* **1983**, *113*, 601. (e) Corradini, P.; Guerra, G.; Barone, V. *Eur. Polym. J.* **1984**, *20*, 1177. (f) Venditto, V.; Guerra, G.; Corradini, P.; Fusco, R. *Eur. Polym. J.* **1991**, *27*, 45. (g) Corradini, P.; Busico, V.; Cavallo, L.; Guerra, G.; Vacatello, M.; Venditto, V. *J. Mol. Catal.* **1992**, *74*, 433.

(26) (a) Arlman, E. J.; Cossee, P. *J. Catal.* **1964**, *3*, 99. (b) Cossee, P. *The Stereochemistry of Macromolecules*; Ketley, A. D., Ed.; Marcel Dekker: New York, 1967; Vol. 1, Chapter 3.

(27) Barino, L.; Scordamaglia, R. *Macromol. Theory Simul.* **1998**, *7*, 407.

(28) Shaka, A. J.; Barker, S. B.; Freeman, R. *J. Magn. Reson.* **1985**, *65*, 355.

(29) Ernst, R. R.; Bodenhousen, G.; Wokaun, A. *Principles of Nuclear Magnetic Resonance in One and Two Dimensions*; Clarendon Press: Oxford, 1987; Chapter 4, pp 474−475.

MA981941N